Increasing throughput in x-ray computed tomography measurement of surface topography using sinogram interpolation

OPEN ACCESS
IOP Publishing
Measurement Science and Technology
Meas. Sci. Technol. **30** (2019) 125002 (12pp)
https://doi.org/10.1088/1361-6501/ab37e5

Increasing throughput in x-ray computed tomography measurement of surface topography using sinogram interpolation

Lars Körner[1,4], Simon Lawes[1], David Bate[2], Lewis Newton[1], Nicola Senin[1,3] and Richard Leach[1]

[1] Faculty of Engineering, Manufacturing Metrology Team, University of Nottingham, Nottingham, United Kingdom
[2] Nikon Metrology UK Ltd., Tring, United Kingdom
[3] University of Perugia, Perugia, Italy

E-mail: Lars.Korner@nottingham.ac.uk

Received 1 February 2019, revised 18 July 2019
Accepted for publication 1 August 2019
Published 16 September 2019

Abstract

X-ray computed tomography (XCT) is a non-destructive imaging technique that has recently gained interest as a tool to measure surface topography. Large acquisition times are a major shortcoming of XCT. One contributing factor to the acquisition time is that a measurement can require the acquisition of thousands of radiographic projections. This paper explores the combined effects of undersampling, i.e. taking fewer radiographic projections and sinogram interpolation, i.e. estimating the missing radiographic projections by interpolation. Different degrees of sinogram interpolation are investigated through the measurement of the surfaces of a metal, additively manufactured part. The quality of the measurement result is assessed via the analysis of the reconstructed volumes, through the computation of quantitative indicators of spatial resolution and noise, and via the analysis of surface topographies extracted from the reconstructed volumes. The quality of the surfaces is assessed through the use of statistical models designed to estimate repeatability errors in the reconstruction, and through the computation of surface texture parameters. Results obtained with no undersampling and no sinogram interpolation are taken as reference. It is shown that noise in the volumetric reconstruction increases with respect to the reference with larger degrees of undersampling, but the increment can be partly compensated by sinogram interpolation with the effects on spatial resolution more difficult to interpret. The computation of surface texture parameters results in similar values for all but one case, the largest undersampling. The topography of the reconstructions indicate that the repeatability error remains similar in all experimental conditions, excluding the case of largest undersampling. Overall, the results indicate that a reduction of the acquisition time of XCT topography measurement is feasible. However, the obtained surface topographies suffer, and large undersampling creates unrecoverable negative effects on the spatial resolution, the noise characteristics and the obtained topographies, even when sinogram interpolation is used.

Keywords: x-ray computed tomography, surface topography measurements, sinogram interpolation

(Some figures may appear in colour only in the online journal)

[4] Author to whom any correspondence should be addressed.

1. Introduction

X-ray computed tomography (XCT) is a non-destructive, volumetric imaging technique. While XCT originated in the medical sector over 50 years ago, the technology has transitioned into the non-destructive engineering sector as a metrological tool for both dimensional and surface metrology [1–3]. The volumetric nature of XCT has led to an interest in applying it on additively manufactured (AM) parts [4], which often feature complex internal geometries. However, XCT has a complex measurement chain, and can be relatively slow when imaging metallic or other highly x-ray attenuating parts. Low photon flux due to high attenuation or low photon flux of the x-ray tube is often associated with an increase in the noise of the reconstructed volume [5], which in turn can cause errors in surface determination [6]. While studying digital filters applicable to the individual projection or to the reconstructed volume, Bartscher *et al* [7] were able to show that the form error of metrological XCT measurements of a calotte cube is reduced when the filters reduce the signal to noise ratio—but the resolution decreased. The concept of losing resolution for a reduction of noise is not limited to digital filters. For example, techniques such as increasing the focal spot size in return for a higher x-ray flux reduce the spatial resolving power of the x-ray system [3]. High resolution is often needed to image voids, surface particles, scratches and sharp corners [8–14]. Hence, it is often necessary to find ways to decrease noise while maintaining a good resolution, which is often achieved by sacrificing the measurement speed.

Low throughput rate in XCT measurement can be attributed to the interaction of several factors. One dominating factor is the exposure time needed to provide sufficient integration time at the detector if a relatively low intensity x-ray source is adopted. A commercial laboratory micro-focus x-ray gun is able to produce an electron beam of a few watts but still will yield a low intensity when compared to non-laboratory based x-ray sources [3]. Noise increases when only a few of the produced x-ray photons reach the detector, which is typically the case for highly attenuating parts. A low intensity source is often counteracted by increasing the exposure time (i.e. integration time) of the detector.

The exposure time for a radiograph is a significant burden when one considers it combined with a further important factor which affects slow throughput rate, i.e. the number of radiographs needed for the reconstruction of a measurement volume. The number of equally spaced angular poses (referred also to as projections or radiographs) needed for an analytical reconstruction of a fan beam system to fully reconstruct a volume can be derived from the discretised form of the central slice theorem [15, 16]. For a 2D reconstruction problem, the central slice theorem states that the 1D Fourier transform of each projection is a slice through the Fourier space of the reconstructed image. Important variables to consider for calculating the number of projections are the maximum object radius and the largest frequency component in the reconstructed volume [17]. For a measurand object whose lateral size fully covers a 2000 by 2000 pixel detector, and whose centre of rotation is in the centre of the detector, the number of projections needed for the fan beam slice to fully sample the object is 3142, assuming the largest frequency component present in the reconstructed volume is limited to the reconstructed voxel size [17]. Reducing this reference number of projections, i.e. undersampling the radon space, will yield to streak artefacts, view aliasing and induce noise in the reconstructed volume [16, 18–21].

Current XCT instrument suppliers have managed to reduce the amount of time associated with each angular pose by continuously rotating the object during the entire scan—as opposed to keeping the object still during the generation of any specific radiograph. However, the continuous motion during capturing a radiograph is associated with a loss of resolution. Any significant movement of the sample during an exposure will lead to a loss of the higher spatial frequencies of a radiograph [22]. The amount of resolution lost when scanning with continuous motion depends on the projected pixel size and the magnitude of the rotation during the generation of the radiograph.

Several techniques have been explored in the medical literature to reduce the number of projections needed for volumetric reconstruction. The most popular approaches are based on the use of iterative reconstruction techniques [23–26]. Iterative reconstruction techniques are often based on repeated forward projection and back projection. Forward projection is the process where the current reconstructed volume is used as the input for a radiograph simulation. Then the interactions between the object and x-rays are simulated to create a 'virtual' projection from the current reconstructed volume. The current reconstructed volume is then updated by adding the virtual projection. The procedure is repeated until some defined convergence criterion is met (see [23–26] for background).

Another technique to reduce the number of projections is sinogram interpolation [27]. Sinogram is the term given to the dataset obtained by stacking a row of each acquired radiograph behind each other, building a 2D space where the second axis is the projection angle (i.e. angular pose). Repeating this for all detector rows, a 3D space is build. The resulting 3D space is sometimes referred to as radon or sinogram space. Sinogram interpolation techniques use the existing radiographs to estimate radiographs at intermediate angular poses. Being an interpolation method, the original data points are not affected and additional ones are created. Clearly, the theoretical advantage of sinogram interpolation is that one could obtain full volumetric reconstructions from a reduced set of radiographs (hence, shorter measurement times), just by computing the missing projections by interpolation. Methods proposed for sinogram interpolation include linear interpolation [20] and Fourier approaches, such as sinc interpolation [28, 29]. The interpolation methods exclusively use the greyscale information in the available radiograph data. In early work from the medical community, it has been observed that, whilst reconstruction artefacts and noise can be reduced by sinogram interpolation, reduction of resolution in the reconstructed volume is also observed [20].

The work presented here explores the effects of sinogram interpolation to increase the throughput of XCT measurement

for the inspection of surface topography, and investigates how such interpolation affects the reconstructed topographies. More specifically, the goal is to assess how sinogram interpolation affects the resolution and noise levels associated with volumetric reconstruction and ultimately propagates through to the topography of the extracted surfaces.

In this work, continuous motion XCT is used to achieve short measurement times. Starting from a complete set of radiographs taken as reference, the use of increasingly smaller subsets of projections is investigated, combined with the application of sinogram interpolation to reconstruct the missing data. Each resulting volume is then used to extract surface topography. The topography datasets are compared in terms of repeatability error and values of surface texture parameters.

2. Methodology

2.1. XCT setup

The XCT system used in this study is a Nikon MCT225. It has a 2000 by 2000 pixel caesium iodide flat panel scintillating detector, with a nominal uniform pixel size of 200 μm. The manufacturer states the maximum permissible error in accordance to the VDI/VDE 2630-1.3 for this system as: $\mathrm{MPE_{SD}} = 9 + \frac{L}{50}$ μm (for the sphere distance characteristic, where L is in millimetres) [30].

The test sample is a Ti-6Al-4V additively manufactured (AM) cube with nominal side length of 10 mm. The sample was manufactured on a laser powder bed fusion system. The raw material used is a sieved powder with grain size below 32 μm. The surface for investigation is the top one, facing upwards in the build direction. The test object is chosen over other possible test objects for the following reasons. The range of non-linear, material and geometry dependent influence factors in XCT is large [31], hence the validity of extrapolation statements between different setups within XCT is often limited. For this case study, an AM surface was chosen, due to the range of scales of features and the complexity of the surface texture [32].

The sample was mounted on a bespoke ABS fixture. The fixture was designed to tilt the sample by 5° with respect to the central slice, see figures 1(b) and (c). The part was scanned at a magnification of approximately 18.7 ×, which yields a projected pixel size of approximately 10.69 μm. The sample was not moved from its fixture between the scans. The gun of the MCT225 was set up with an acceleration voltage of 190 kV and a filament current of 53 μA. According to the manufacturer's specification, this leads to an apparent focal spot size smaller than the projected pixel size. The spectrum produced by the cooled tungsten target was filtered sequentially by 0.5 mm copper, then by 0.5 mm aluminium. The detector exposure time was set to 2000 ms, and two exposures were taken and averaged to obtain a radiograph. Before performing each scan, a two-point white level correction was performed. The white level correction contained 128 radiographs in the fully exposed condition and the same number of radiographs were taken for the dark reading. All the collected radiographs were corrected for variations in the x-ray flux by Nikon's flux normalisation tool. The temperature of the XCT cabinet is actively controlled to 20 °C ± 0.5 °C by the MCT225, and the x-ray gun temperature is monitored by thermocouples at several locations. The XCT was set to measure with the part in continuous rotation.

Each reconstruction was performed in Nikon's CT PRO software. No beam hardening correction was applied to any of the data sets. The same reconstruction settings were applied to all the data sets. No additional filtering was applied during, before or after the reconstruction other than the reconstruction filter. The reconstruction filter was a basic ramp-filter and was the same for all experimental conditions. The angular position of each radiograph was derived by assuming equal spread around 360°. The machine manufacturer tool to calculate a sub-voxel location of the centre of rotation was used.

2.2. Sinogram interpolation

The Whittaker–Shannon interpolation method, also known as sinc interpolation [33], was used in this work. Sinc interpolation is based on inserting additional zero components into the discrete Fourier space of the sinogram. The number of zeros needed can be derived from the relationship between Fourier space points and spatial points. Because of memory limitations of the available computer hardware for this work, the volume was split into two sub-volumes of equal size, which were processed separately. Each sinogram slice of each sub-volume was then interpolated independently; see figures 2(a)–(c) for an example of the interpolation process.

2.3. Experiments

For this setup, the number of projections was calculated as 3142, given the number of detector pixels and assuming that the sample fully covers the field of view (FoV). Five test conditions were considered, each consisting in measuring the sample with a decreasing total number of projections corresponding to 80%, 60%, 40% and 20% of the theoretical reference number. For each test condition, three measurements were performed with identical setup (repeatability conditions). Then, each sinogram was upsampled by different amounts in order to match all the previous downsampling levels up to no downsampling, i.e. the reference number 3142. So, for example, the three measurements realised with 40% of the reference theoretical number of projections (1257 projections) were upsampled at 1885 (60%), 2514 (80%) and 3142 (100%) projections. The full set of experiments and the naming conventions used are summarised in table 1. The acquisition times of 628 projections was around 42 min, around 84 min for 1257 projections, around 126 min for 1885 projections, around 168 min for 2514 projections and 3142 projections required around 209 min. The interpolation of ORG628 UP3142 needed around twelve min, and the upsampling of ORG2514 UP3142 required approximately 21 min (elapsed time using non-compiled code on an Intel Xeon E5 processor).

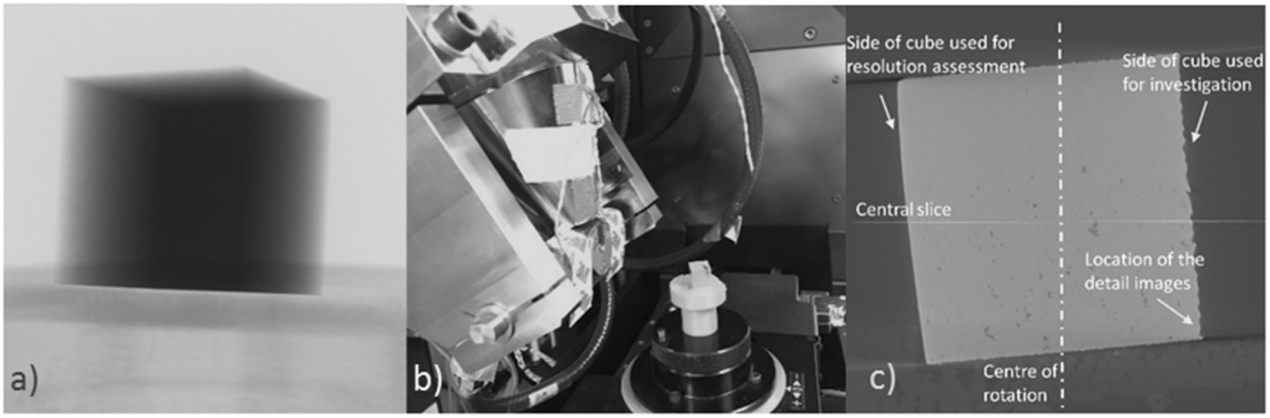

Figure 1. (a) One of the radiographs acquired, (b) a view of the sample in the XCT system, and (c) a reconstructed slice.

Table 1. Experiments, indicating conditions and naming convention.

Original experimental data						
100% of projections required: 3142	80% of projections required: 2514	60% of projections required: 1885	40% of projections required: 1257	20% of projections required: 628		
ORG3142	ORG2514 UP3142	ORG1885 UP3142	ORG1257 UP3142	ORG628 UP3142	3142	Number of projections used in reconstruction
—	ORG2514	ORG1885 UP2514	ORG1257 UP2514	ORG628 UP2514	2514	
—	—	ORG1885	ORG1257 UP1885	ORG628 UP1885	1885	
—	—	—	ORG1257	ORG628 UP1257	1257	
—	—	—	—	ORG628	628	

2.4. Topography comparison

The reconstructed volume datasets were imported into VGStudio Max 3.0, where the surface determination was performed using the advanced surface determination method. The surface determination method was set to operate at a search distance of four voxels. In addition, the software was instructed to 'remove particles and all voids' setting (i.e. removal of small, topologically disconnected portions of the surface appearing as floating particles and voids). The final surfaces were exported into STL meshes using default settings.

To evaluate sinogram interpolation effects on surface topography, a region of interest highlighted in figure 1(c)) was selected and extracted from all STL meshes. The STL datasets were aligned to a common reference, which was selected as the surface region extracted from ORG3142, the dataset obtained by using the reference number of projection and no sinogram interpolation. The alignment was based on the application of the iterative closest point (ICP) method, as described in [34]. Again following the comparison procedure described in [34], the aligned datasets were raster scanned into 2.5D height maps ($z = f(x, y)$ functions, with z values at discrete x, y positions distributed on a regular x, y grid). Point spacing in the x, y grid was chosen as approximately 5 μm, as it matches closely to half of the reconstructed voxel size.

The height maps were then transferred into the surface metrology software MountainsMap [35] for the computation of ISO 25178-2 areal field surface texture parameters [36]. Parameters were calculated on an extracted area of (4×4) mm; levelled by least squares mean plane subtraction; S-filter of nesting index 12 μm; L-filter of nesting index 800 μm.

In addition to the comparison of texture parameters, a comparison was performed on the actual reconstructed topographies by applying the method described in [37]. This method consists of creating a statistical model of topography from multiple measurements in repeatability conditions, and then comparing the statistical models corresponding to different set-ups with each other (in this case, different downsampling and sinogram interpolation levels), to assess the overall amount of discrepancy between set-ups. Each statistical model is comprised of a mean topography, estimated from the repeated measurements, and an indication of local scattering of the data, estimated through local confidence intervals on the mean (at 90% confidence level), visualised through upper-bound and lower-bound surfaces (further details can be found in [34]). In this work, the amount of discrepancy between statistical topography models corresponding to each experimental condition was reported as a discrepancy ratio, i.e. the percentage of surface points where the confidence intervals on the local means do not intersect. In addition, the arithmetic mean of the distance between the upper and lower bound surfaces for each statistical topography model was computed, as an overall measure of repeatability error in surface determination in each experimental condition.

2.5. Volume data: noise

The Shannon entropy, applied to the reconstructed volume, was used to quantify the amount of noise associated with each experimental set-up. This decision was made based on the work of Schienlein *et al* [38], where the authors were able

to show a better agreement between the occurrence of image artefacts than by using signal-to-noise ratio. The Shannon entropy uses the histogram data of the entire reconstructed volume, and is defined as [38]:

$$H := -\sum_{i=1}^{N} p_i \log_2 p_i \tag{1}$$

where p_i is the probability of a voxel value to fall within the ith histogram bin and N is the total number of histogram bins. As Shannon entropy increases with wider distributions, small Shannon entropy values indicate low levels of noise [38]. In this work, histograms with 2^{16} data bins were exported from VG Studio 3.0.

2.6. Volume data: resolution

Different concepts of resolution have been introduced in the literature of ditigal image analysis/processing in general, as well as for XCT metrology, such as high and low contrast resolution [19], structural and positional resolution [3, 39]. Notable approaches to determine resolution include the 'multi-wave standard' [10], the hour glass approach [40] and radius-based approach [41].

In this work, an approach was adopted where resolution of the volume data is estimated by investigating the image sharpness between background and material. The approach is an adaptation of the original method described in ISO 12233 for photography [42]. For the purpose of the method, one of the side surfaces of the test sample was polished in order to have negligible texture at the adopted XCT measurement magnification. For each experimental set-up, the transition was evaluated on a cross-section extracted from the reconstructed volume (figures 1(c) and 5(a)). Since the test sample is oriented with a tilt of 5° at measurement, the edge in the cross-section appears slanted with respect to the pixel grid. An example of pixel intensities in the transition between background and material is shown in figure 5(b) for one of the measurements; the edge spread function is obtained by aligning and averaging multiple rows of pixels of the cross-sectional image with oversampling. Resolution can be defined as the width of the transition region from the reference intensity values for the background, to the reference intensity value for the material (see later). Such a width is here referred to as edge spread. A more robust edge spread can be obtained by repeating the computation over a number of parallel lines drawn on the cross-sectional image, aligning them and by finding their arithmetic average [42].

As the method operates directly on the pixels of the cross-sectional image extracted from the reconstructed XCT volume, it should be noted that the method ignores the surface determination stage. It should also be pointed out that the method to assess resolution is only meant to provide values for comparison use, i.e. it does not provide an absolute value. The void and material reference pixel intensity levels, needed for computing the edge spread, were computed as follows. Due to the likely presence of beam hardening, an initial material intensity value was determined by averaging pixel intensities at a large distance from the visible edge. The same process was used to determine an initial estimate of the background intensity value. These two initial values were referred to as the 0% (background) and the 100% (material) intensities in the surroundings of the transition. Then, the transition range was narrowed by using the 10% and the 90% levels of the previous range as the final thresholds to identify the transition and compute its width in voxels [43]. Failed readings of this method, identified by a skewed or noisy edge spread function, were ignored and repeated. For each of the three repeats of each experimental condition, ten edge spread computations were performed. After an initial user input of the location along the edge, the remaining nine edge spread computations were chosen randomly within twenty pixels around the initial user selection. The thirty edge spread computations obtained from each experimental condition were used to obtain an arithmetical mean edge spread. The associated scatter was quantified as the distance between the minimum and maximum edge spread value over 30 repeats.

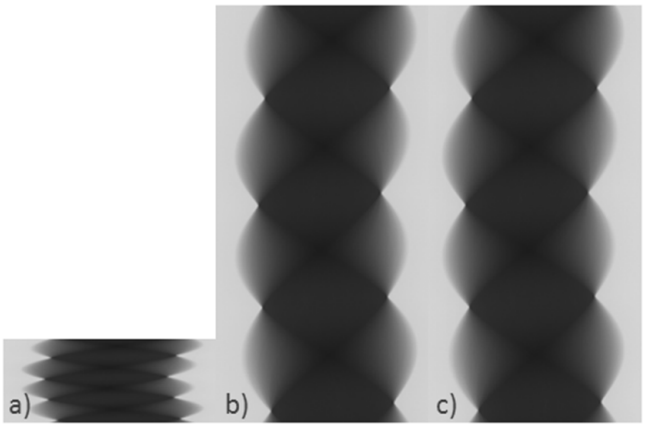

Figure 2. Three 2D central slices of three different sinograms are shown. The sinograms are (a) ORG628, (b) ORG3142 and (c) ORG628 UP3142. While all three sinogram slices represent 360° rotation, for visualisation the pixel in the direction of rotation, the vertical axis, are not stretched and the pixel representations is kept square.

3. Results

The results section is split into four subsections each discussing one of the following themes: noise, resolution, areal texture parameters, and comparison via statistical topography models. Figure 4 shows a selection of the details of reconstructed slices for some of the experimental conditions. Figure 3 shows the statistical topography models obtained for the experimental conditions described in section 2. The statistical topography models also allow for one fundamental consideration, based on simple visual inspection: the amount of noise is reduced when increasing the number of projections from which the interpolation starts. This can be understood by observing the spikes in the green surfaces, which are the upper bounds of the local confidence intervals computed on triplicate data points, as illustrated in section 2. Each spike corresponds to a local confidence interval larger than the neighbouring

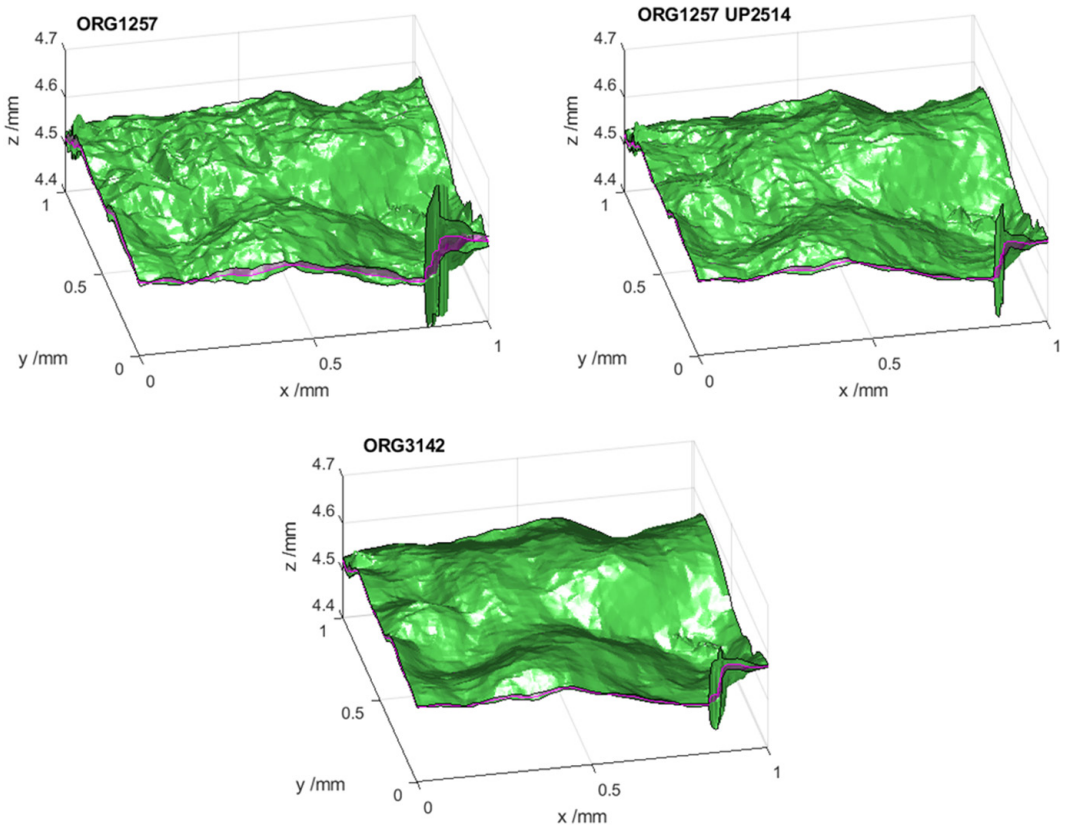

Figure 3. Statistical topography models from the repeated measurements (triplicates) for each experimental condition. Three experimental conditions (set-ups) are reported. For each: the top, green surface is the upper limit of the local confidence interval of the mean and the lower surface the lower bound. The upper bound is highlighted by a black line at the sides of the region considered. The purple surface, also visible at the sides, is the mean topography.

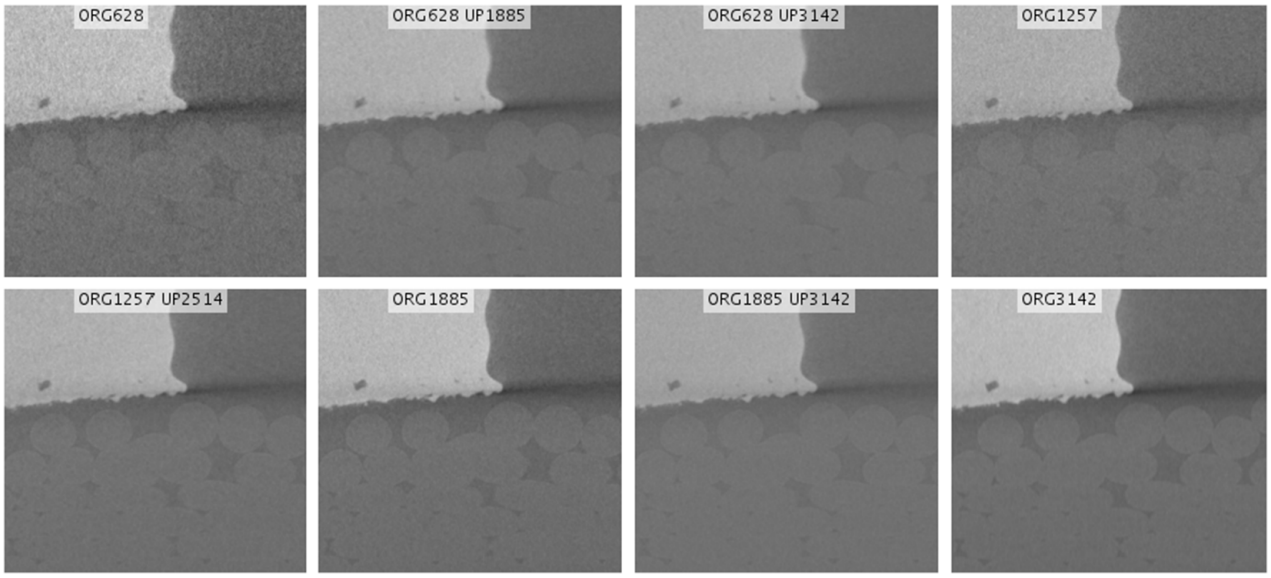

Figure 4. A collection of details of various reconstructed data sets. The location of detail is highlighted in figure 1(c). The variation in noise between the different experimental conditions can be observed. All images were intended to have similar grey scale distributions, by manual manipulation of the transfer function of VG Studio.

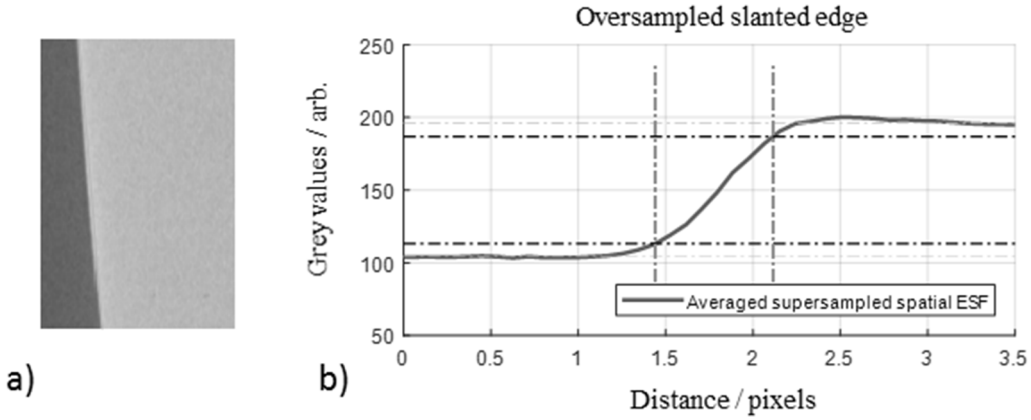

Figure 5. (a) A reconstructed cross sectional image of the slanted edge. (b) The oversampled edge spread function, and graphical indication of how the 10% to 90% value is found.

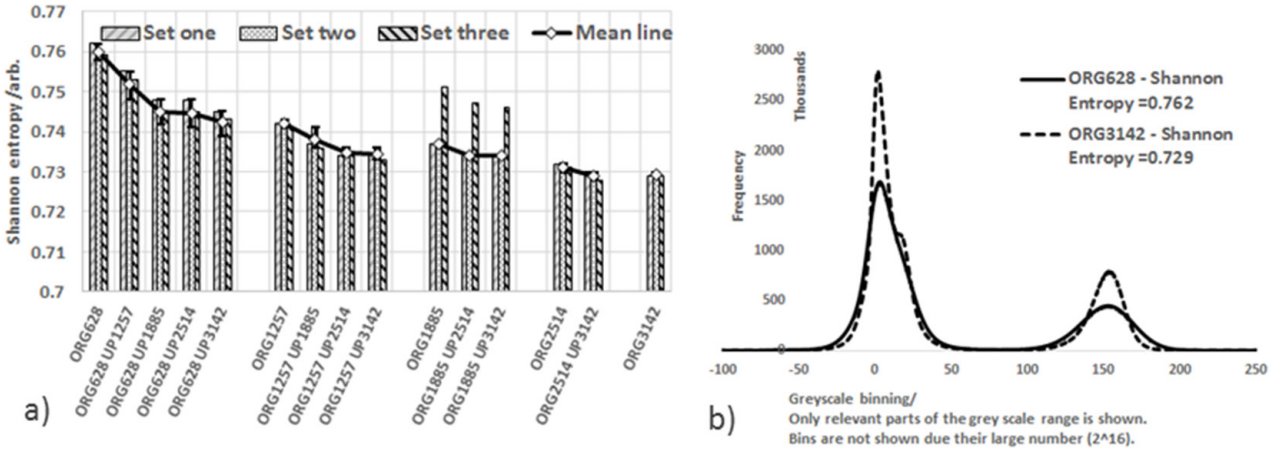

Figure 6. (a) Shannon entropy values for the experimental conditions (mean and range from three repeats). The experiments are ordered by the total number of projections used in the reconstruction. (b) Two example histograms of reconstructed volumes.

ones, indicating a larger spread of the data points at the same location, i.e. larger noise.

3.1. Noise in the reconstructed volume

The histograms of the voxel intensities of two example scans are shown in figure 6(b). Qualitatively inspecting the two histograms of figure 6(b), the contrast, i.e. the separation in the grey scale between the reference value of material and background, of both distributions coincide well as expected. Comparing the two histograms, the histogram of only 628 projections shows a wider and flatter shape of the material and background peaks, which is generally attributed to nosier datasets.

The Shannon entropy was computed and is shown in figure 6(a). The data sets of the third repeat of ORG1885 and its interpolated variants show outlier behaviour, hence they were excluded from further processing. Due to operational reasons, the system had to be shut down before the last set of repeats could be acquired. The sample was not moved and an additional warmup scan of over two hours was added before commencing the remaining scans. The first scan after the second warmup was the final repeat of ORG1885, thus it is considered an outlier. The repeatability between Shannon entropy values for the different repeats of each experimental condition was high, with a maximum difference limited to less than 1% of the Shannon entropy value. Despite reducing the Shannon entropy, sinogram interpolation does not reach the same low level of noise achievable by acquiring the actual number of projections without interpolation. Also, while the error bars provide some indication of the spread of the entropy results, clearly a higher number of repeats would be beneficial for improving confidence.

3.2. Resolution in the reconstructed volume

The values shown in figure 7 are the mean values of the resolution, obtained as described in section 2.5, for the three repeats of each experimental condition and ten edge spread computations per repeat. This yields thirty edge spread measurements per experimental condition, and the error bars are the maximum spread of the thirty repeats.

The range of the obtained resolution values is large, even within each experimental condition. All upsampled versions

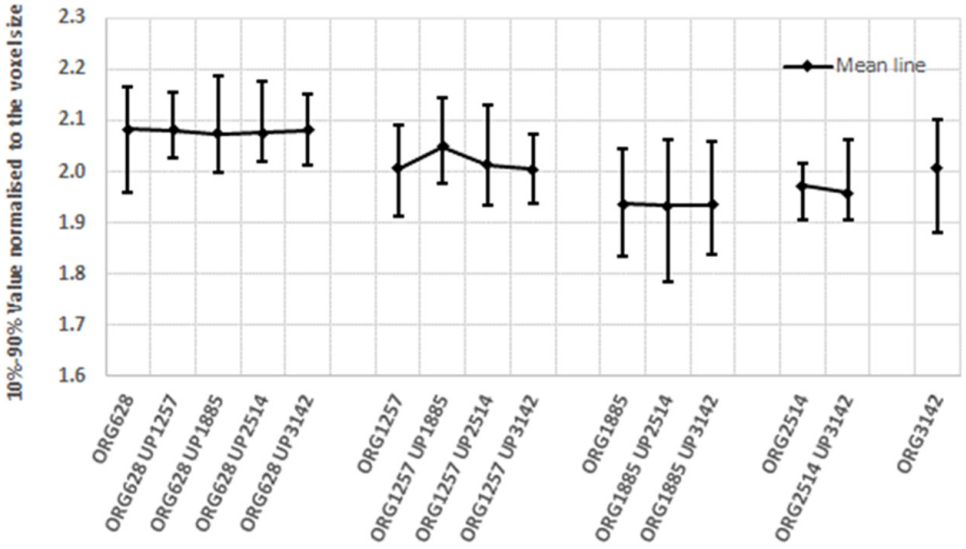

Figure 7. (a) Mean values of the resolution estimate via edge spread determination. The error bars show the spread from 30 repeats, which are ten edge spread computations per each reconstructed data set.

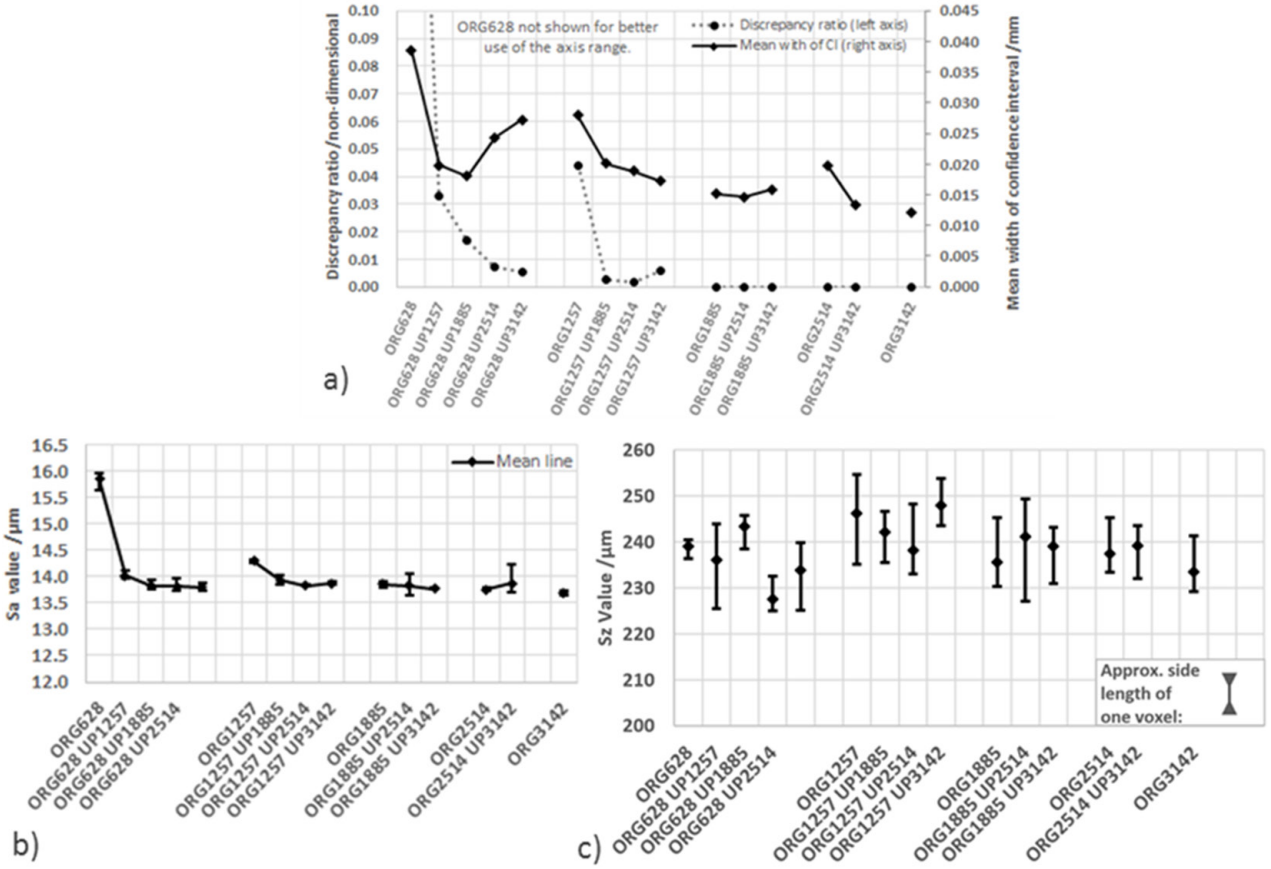

Figure 8. (a) Discrepancy ratio between each experimental condition and ORG3142. The second axis to the right of the panel shows the mean width of the confidence intervals; (b) mean *Sa* value and its min-max range over three replicates; (c) mean *Sz* value and its min-max range over three replicates. For (b) and (c) the error bars show the maximum range of the data.

of ORG1885 showed lower resolution values than ORG3142, but within the margins of the error bars. The ORG1885 was also the test sample which showed outlier behaviour in the Shannon entropy. The results indicate that a large angle during the continuous motion will worsen the resolution. However, no trends are particularly prominent in the collected data.

3.3. Discrepancy and repeatability error in the extracted surface topography

In addition to the already discussed visual inspection of the results shown in figure 3, statistical topography models allowed for quantitative comparison between experimental conditions. Figure 8(a) shows both the discrepancy ratio and

the mean confidence interval height of each experimental condition. The results of the discrepancy ratio are zero for any experimental condition after ORG1885 in figure 8(a), and zero for ORG3142 by design.

3.4. Areal texture parameters

The results for the areal surface texture parameters *Sa* and *Sz* [44, 45] are shown in figures 8(c) and (d) respectively. The mean values of the parameters over three replicates are reported, together with error bars representing the min-max range. Notice that *Sa* was chosen as an indicator of the average spread of surface height values about a mean reference. On the contrary, *Sz* was chosen as an indicator of the min-max range of height values, so it should be considered more sensitive to extreme values.

4. Discussion

XCT measurements can be relatively slow and a method to decrease acquisition time has been explored in this paper. The method is based on using a reduced number of projections in combination with sinogram interpolation. As undersampling is known to increase noise and streak artefacts, the questions to answer in the discussion are related to the capability of sinogram interpolation to reduce such effects. In particular: can the noise be reduced? How much does the resolution suffer? Are there any noticeable effects on the reconstructed topography? And ultimately, is it possible to recommend an optimal combination of undersampling and interpolation to obtain a reasonable compromise between time gain, noise level and loss of resolution?

Initially, it was the authors' intention to use the obtained height map data to calculate the spatial frequency content of the measured topographies, in particular focusing on the high-frequency content as a means to obtain a qualitative assessment of the capability of capturing small-scale topographic detail. However, the presence of noise rendered this approach impractical. While not within the scope of this paper, it is anticipated that similar problems will occur when using frequency-based resolution test-artefacts, such as in [10].

Figure 6(a) showed a strong trend of decreasing noise with increasing amounts of interpolation, as measured by the Shannon entropy. The noise in the ORG datasets is expected to change dramatically as the number of photons recorded is different. In fact, if one were to think of the number of photons per voxel, a common helpful quantity when comparing scans, the ORG628 will obviously only equate to 20% of the energy recorded by the detector, which is a significant reduction. For example, the large degree of noise in ORG628 was significantly reduced by interpolation, even by upsampling to only 1257 projections. In all cases, the upsampling of each originally undersampled set of projections led to reduced noise. When comparing all the experimental conditions, the ORG3142 and the ORG2514 UP3142 sets were the ones which showed the best results. Excluding the outlier represented by the third ORG1885 set, the low repeatability error of the Shannon entropy results also supported the significance of the results. As can be seen in figure 6(a), ORG1257 UP3142 achieved similar noise behaviour to the upsampled versions of ORG1885 series. However, the best noise behaviour is achieved when acquiring a full set of projections, closely followed by ORG2514 UP3142.

The measurement procedure adopted to estimate the resolution of the different scans is based on the assessment of edge spread. The authors are aware that this method does not represent the entire measurement chain, but is limited to the analysis of a single slice of the reconstructed volume. However, at least it can be noted that pixel intensities are the usual input to the surface determination stage. The conclusions that can be drawn from these results are of difficult to summarise, due to the large error bars which yield no experimental condition showing any significant difference in resolution. The error bars were chosen conservatively as the maximum spread, rather than the standard deviation. The experimental campaign should be expanded with further experimentation on how the edge spread method of measuring resolution is affected or even confounded by noisy data, and the repeatability of this method needs further attention, such as exploring alternative methods [7, 10, 41, 46, 47]. Despite the issue of not having detected significant variations of resolution, one can at least conclude that resolution does not degrade to an extent that can be adequately captured with the adopted edge spread method. However, the authors do also believe that the extents of resolution degradation should be worse, at least based on the findings of the medical literature [20, 33]. The discrepancy could be due to the different nature of the sinogram space of a multi-material object, such as when scanning a human body, compared to the single-material object presented in this work, but more detailed experimental and analytical work on how the interpolation propagates into the reconstructed volume is needed. In summary, not much confidence is given to the resolution measures obtained within this study. In the wider scope of comparing measurement setups of XCT, a reliable and sensitive method of expressing the achieved resolution is needed.

Furthermore, given the angular motion, it could be expected that the resolution will vary depending on the radius around the centre of rotation. The design of the fixture for the part assured that the investigated surface topography and the flat side used for investigation into the resolution are approximately at the same radial distance from the axis or revolution (see figure 1). However, it would be interesting to study the isolated effects of continuous motion, the nature of the motion blurring and its practical limits for faster acquisitions.

Overall, the results indicate that the application of sinogram interpolation to a reduced number of projections holds promise for the field of topography measurements via XCT and indeed for dimensional measurements. The *Sa* texture parameter is not affected greatly once more than 628 projections are used for the reconstruction. In general, the *Sz* results are in similar regions for all experimental conditions, though *Sz* is a very sensitive parameter to outliers as it describes the maximum range of the height map data. Interestingly, the experimental condition which showed the most repeatable *Sz*

value is the ORG628. Putting the obtained mean Sz values into perspective to the voxel size, the results still deviate by approximately three times the voxel size, and the spread of Sz of each test condition is larger still at approximately six times the voxel size.

The more interesting conclusions can be drawn from the numerical topography comparison, which is depictured in figure 8(a). Figure 8(a) shows the discrepancy ratio of each experimental condition with respect to the ORG3142 condition (taken as reference) and the mean width of the confidence interval calculated for each experimental condition aligned to ORG3142. The resultant mean confidence interval width is of the order of tens of micrometres. One interesting feature has been identified for ORG628 UP2514 and ORG628 UP3142. Here, the discrepancy ratio to ORG3142 is reduced, while the mean width is increased. This is can be explained as the discrepancy ratio will reduce if the confidence interval is large—as there is more chance for overlap. The cause of the increase of the confidence interval can possibly be attributed to a loss of resolution. Both ORG628 UP2514 and ORG628 UP3142 have the largest upsampling ratios, which is four and five respectively. This might indicate that too much upsampling has occurred and might affect the quality of the obtained surface topography data.

The discrepancy ratio drops to zero, for all cases which are based on 1885 real projections or more—while maintaining mean confidence interval widths of around ten to twenty micrometres. This finding may indicate that a reduced number of projections is feasible. However, the effects of interpolation are not dramatic for the cases which are based on more than 1885 projections. While ORG1257 has large mean confidence interval width, and a large discrepancy ratio, a substantial improvement can be seen when increasing the number of projections used in reconstruction to 1885. However, the case of ORG1257 UP3142 shows an increase in the discrepancy ratio compared to ORG1257 UP2514. Most experimental test conditions do not reach the same confidence interval mean width levels as ORG3142. Overall, the interpolation in ORG1257 seems to be promising, however, it would be interesting to explore the loss of resolution in more detail, and compare the interpolation against more computationally expensive reconstruction processes, such as iterative techniques [48], but also against other filtering methods on the volume data, on which initial work has been started [29].

Some observed limitations need to be discussed. It is clearly observable that even in ORG3142, i.e. the reference measurement, some noise was present. It could be possible that further adjustments in the XCT measurement parameters can reduce the noise. The authors are hoping to perform a further simulation-based study, to remove the influence of photon noise. Further, only three repeats were performed per experimental set-up, and the data obtained from one repeat is visibly worse than the other two. This means that within the context of drawing a conclusion of the presented data, the statistical validity and confidence is limited. This is a common issue in XCT metrology where, somewhat ironically, repeated measurement is rarely used due to lengthy measurement times. The experimental campaign included three repeats, without moving the sample. But no investigation was undertaken into the reproducibility of this experimental findings, and how the reproducibility relates to the observed outlier. The statistical surface model currently only considers uncertainty attributed to the z-axis and currently excludes the localisation error of the x, y directions. Part of the x, y error is compensated by the lateral alignment procedure, which we implement to construct the statistical model, but of course this cannot take into account for all error components.

Further, only one test sample was investigated. While the test sample was chosen as a typical application, the experimental activities described in this work were not tested on a wider range of scenarios, including different geometries, topographies and materials. How and if these findings can be extrapolated needs further investigation.

So, which experimental condition should be recommended to increase the throughput rate? All data derived from ORG628 should be immediately excluded as they showed on average a much worse performance in terms of noise, and even more importantly they showed a significant difference from the reference measurement in terms of the discrepancy ratio.

Both ORG1885 UP2514 and ORG1257 UP2514 do not perform worse than their respective counterparts which used 3142 in the reconstruction, in terms of noise. ORG2514 and its upsampled partner only decreased the measurement time by approximately 20%, while slightly outperforming the ORG1257 UP 2514 and ORG1885 UP 2514 in terms of Shannon entropy. The most important findings though are shown in graphs on the numerical topography comparison in figure 8. The topography comparison showed that the ORG1885 UP2514 achieved similar results to the ORG3142 in terms of the mean width of the confidence interval and has a zero discrepancy ratio. However, ORG1257 UP2514 does have a larger mean width of the confidence interval and does have discrepancy ratio, but reduced the measurement time by 60%. While the overall recommendation depends on how much of the fidelity and speed is needed, both the ORG1885 UP2514 and ORG1257 UP2154 cases are promising candidates.

5. Conclusions

This paper explored the possibility to reduce the number of acquired projections in XCT measurements of surfaces, by applying sinogram interpolation. The different experimental conditions were compared and characterised in terms of noise, resolution and a direct comparison of the obtained surface topographies. Sinogram interpolation was applied to data sets which were undersampled by 20%, 40%, 60% and 80% of the analytically required number of projections. The XCT system was set up to rotate continuously during acquisition to keep the time associated with each radiograph low. An additively manufactured test cube was used as a test sample. The method for assessing resolution showed limits when capturing the resolution changes between the various configuration setups. Noise was found to worsen with increased undersampling (decreased number of projections) but it could be reduced by sinogram interpolation. The topography comparison showed

that sinogram interpolated versions of the cases which used 40% and 60% of the required radiographs, had a strong potential of delivering the information needed, while also reducing the acquisition time significantly. However, the limitations of these findings should be considered carefully as the extrapolation is limited due to the feature size as a function of voxel size, the use of only a single material case and the statistical limitations of having only three repeats. Overall, the findings here show that there is a potential for increasing the throughput time of topography measurement—as long as the user is aware of the additional limitations added by reducing the number of projections and introducing interpolation.

Acknowledgments

This work was supported by the Engineering and Physical Sciences Research Council (Grant Nos. EP/L01534X/1 and EP/M008983/1) (EPSRC). Further, the authors would like to disclose that funding has been received from Nikon Metrology UK Ltd.

ORCID iDs

Lars Körner https://orcid.org/0000-0002-9273-4313
Lewis Newton https://orcid.org/0000-0002-8961-9605

References

[1] Kruth J P, Bartscher M, Carmignato S, Schmitt R, De Chiffre L and Weckenmann A 2011 Computed tomography for dimensional metrology *CIRP Ann.—Manuf. Technol.* **60** 821–42
[2] Townsend A, Pagani L, Scott P and Blunt L 2017 Areal surface texture data extraction from x-ray computed tomography reconstructions of metal additively manufactured parts *Precis. Eng.* **48** 254–64
[3] Carmignato S, Dewulf W and Leach R K 2018 *Industrial X-Ray Computed Tomography* (Cham: Springer)
[4] Thompson A, Maskery I and Leach R K 2016 X-ray computed tomography for additive manufacturing: a review *Meas. Sci. Technol.* **27** 072001
[5] Barret H H and Swindell W 1981 *Radiological Imaging: The Theory of Image Formation, Detection, and Processing* vol 1 (New York: Academic)
[6] Lifton J J, Malcolm A A and McBride J W 2015 On the uncertainty of surface determination in x-ray computed tomography for dimensional metrology *Meas. Sci. Technol.* **26** 35003
[7] Bartscher M, Staude A, Ehrig K and Ramsey A 2012 The influence of data filtering on dimensional measurements with CT *18th World Conf. on Nondestructive Testing (Durban, South Africa)* pp 1–13
[8] Bartscher M, Bremer H, Birth T, Staude A and Ehrig K 2012 The resolution of dimensional CT—an edge-based analysis *iCT2012: Conf. on Industrial Computed Tomography (Wels, Austria)* pp 191–201
[9] Pyka G, Kerckhofs G, Schrooten J and Wevers M 2013 The effect of spatial micro-CT image resolution and surface complexity on the morphological 3D analysis of open porous structures *Mater. Charact.* **87** 104–15
[10] Arenhart F A, Nardelli V C and Donatelli G D 2015 Characterization of the metrological structural resolution of CT systems using a multi-wave standard *XXI IMEKO World Congress 'Measurement in Research and Industry' (Prague, Czech Republic)* pp 1–6
[11] Landstorfer P and Hiller J 2017 Strategies to improve the spatial resolution in micro computed tomography imaging *iCT2017 7th Conf. on Industrial Computed Tomography (Leuven, Belgium)* p 1
[12] Fleßner M, Vujaklija N, Helmecke E and Hausotte T 2014 Determination of metrological structural resolution of a CT system using the frequency response on surface structures *Report* Physikalisch-Technische Bundesanstalt (https://doi.org/10.7795/810.20150223B)
[13] Maskery I, Aboulkhair N T, Corfield M R, Tuck C, Clare A T, Leach R K, Wildman R D, Ashcroft I A and Hague R J M 2016 Quantification and characterisation of porosity in selectively laser melted Al–Si_{10}–Mg using x-ray computed tomography *Mater. Charact.* **111** 193–204
[14] Hermanek P and Carmignato S 2017 Porosity measurements by x-ray computed tomography: Accuracy evaluation using a calibrated object *Precis. Eng.* **49** 377–87
[15] Rattey P A and Lindgren A G 1981 Sampling the 2D radon transform *IEEE Trans. Acoust.* **29** 994–1002
[16] Hsieh J 2009 *Computed Tomography* (Bellingham, WA: SPIE Press)
[17] Joseph P M and Schulz R A 1980 View sampling requirements in fan beam computed tomography *Med. Phys.* **7** 692–702
[18] Barret H H and Swindell W 1981 *Radiological Imaging: The Theory of Image Formation, Detection, and Processing* vol 2 (New York: Academic)
[19] Kalender W A 2000 *Computed Tomography: Fundamentals, System Technology, Image Quality, Applications* (Weinheim: Wiley)
[20] Weiss G H, Talbert A J and Brooks R A 1982 The use of phantom views to reduce CT streaks due to insufficient angular sampling *Phys. Med. Biol.* **27** 1151–62
[21] Barrett J F and Keat N 2004 Artifacts in CT: Recognition and avoidance *RadioGraphics* **24** 1679–91
[22] Cant J, Palenstijn W J, Behiels G and Sijbers J 2015 Modeling blurring effects due to continuous gantry rotation: application to region of interest tomography *Med. Phys.* **42** 2709–17
[23] Hansen P C and Saxild-Hansen M 2012 AIR tools—a MATLAB package of algebraic iterative reconstruction methods *J. Comput. Appl. Math.* **236** 2167–78
[24] Beister M, Kolditz D and Kalender W A 2012 Iterative reconstruction methods in x-ray CT *Phys. Medica* **28** 94–108
[25] Batenburg K J and Sijbers J 2011 DART: A practical reconstruction algorithm for discrete tomography *IEEE Trans. Image Process.* **20** 2542–53
[26] Hsieh J, Nett B, Yu Z, Sauer K, Thibault J-B and Bouman C A 2013 Recent advances in CT image reconstruction *Curr. Radiol. Rep.* **1** 39–51
[27] Hsieh J 2001 B1: Methods and apparatus for FOV-dependent aliasing artifact reduction *US Patent* US6529574
[28] Hsieh J, Slack C L, Dutta S, Gordon C L III, Li J and Chao E 2001 Adaptive view synthesis for aliasing artifact reduction *Proc. SPIE* **4320** 673–80
[29] Körner L, Lawes S, Newton L, Senin N, Bate D and Leach R 2019 Sinogram interpolation to decrease acquisition time in x-ray computed tomography measurement of surface topography *iCT2019 9th Conf. on Industrial Computed Tomography (Padova, Italy)*
[30] Nikon Metrology NV 2018 nikonmetrology.co.uk
[31] Welkenhuyzen F, Kiekens K, Pierlet M, Dewulf W, Bleys P and Voet A 2009 Industrial computer tomography for dimensional metrology: overview of influence factors

and improvement strategies *4th Int. Conf. on Optical Measurement Techniques (Antwerp, Belgium)* pp 1–9
[32] Townsend A, Senin N, Blunt L, Leach R K and Taylor J S 2016 Surface texture metrology for metal additive manufacturing: a review *Precis. Eng.* **46** 34–47
[33] Galigekere R, Wiesent K, Mertelmeier T and Holdsworth D W 2000 On intermediate view estimation in computed tomography *Circuits Syst.* **19** 279–99
[34] Thompson A, Senin N, Giusca C and Leach R K 2017 Topography of selectively laser melted surfaces: a comparison of different measurement methods *CIRP Ann.—Manuf. Technol.* **66** 543–6
[35] Digital Surf Mountains® France 2017
[36] ISO 2012 ISO 25178-2:2012 *Geometrical Product Specifications (GPS)—Surface Texture: Areal—Part 2: Terms, Definitions and Surface Texture Parameters* (Geneva: The International Organization for Standardization)
[37] Thompson A, Senin N, Maskery I, Körner L, Lawes S and Leach R K 2018 Internal surface measurement of metal powder bed fusion parts *Addit. Manuf.* **20** 126–33
[38] Schielein R, Schröpfer S, Kiunke M, Zabler S and Kasperl S 2014 Quantitative evaluation of CT Images by means of Shannon Entropy *11th European Conf. on Non-Destructive Testing (Prague, Czech Republic)* pp 2–4
[39] Verein deutscher Ingenieure e.V. 2014 *Computed Tomography in Dimensional Measurment Fundamentals and Definitions VDI/VDE 2630-1.1 Draft* (Berlin: Verein Deutscher Ingenieure eV)
[40] Carmignato S, Pierobon A, Rampazzo P, Parisatto M and Savio E 2012 CT for industrial metrology-accuracy and structural resolution of CT dimensional measurements *iCT2012 2nd Conf. Industrial Computed Tomography (Wels, Austria)*
[41] Illemann J, Bartscher M, Jusko O, Härtig F, Neuschaefer-Rube U and Wendt K 2014 Procedure and reference standard to determine the structural resolution in coordinate metrology *Meas. Sci. Technol.* **25** 64015
[42] British Standards Institution ISO 12233:2017 2017 *Photography—Electronic Still Picture Imaging—Resolution and Spatial Frequency Responses* (London: The British Standards Institution)
[43] Smith S W 2013 *Digital Signal Processing a Practical Guide for Engineers and Scientists* (Burlington: Newnes)
[44] ISO 2012 ISO 25178 *Geometrical Product Specifications (GPS)—Surface Texture: Areal—Part 3: Specification Operators* (Geneva: The International Organization for Standardization)
[45] Leach R K 2014 *Fundamental Principles of Engineering Nanometrology* (Oxford: William Andrew)
[46] Carmignato S 2012 Accuracy of industrial computed tomography measurements: Experimental results from an international comparison *CIRP Ann.—Manuf. Technol.* **61** 491–4
[47] Thalmann R, Spiller J, Küng A and Jusko O 2012 Calibration of Flick standards *Meas. Sci. Technol.* **23** 1–7
[48] van Aarle W, Palenstijn W J, Cant J, Janssens E, Bleichrodt F, Dabravolski A, De Beenhouwer J, Joost Batenburg K and Sijbers J 2016 Fast and flexible x-ray tomography using the ASTRA toolbox *Opt. Express* **24** 25129